

Scale Dependence of Monsoonal Convective Systems over the Indian Ocean*

RÉMY ROCA[†] AND V. RAMANATHAN

Center for Cloud Chemistry and Climate, Scripps Institution of Oceanography, La Jolla, California

(Manuscript received 12 November 1998, in final form 22 May 1999)

ABSTRACT

Deep convective clouds in the Tropics have long been recognized to occur on a wide spectrum of spatial scales, ranging from the individual cumulus to the meso- and synoptic-scale cloud systems. The objective of this paper is to examine the scale dependence of the properties of clouds embedded in the Intertropical Convergence Zone.

The Indian Ocean during the winter and summer monsoons offers an ideal domain to undertake this study, which uses *INSAT-1B* infrared imagery. The cloud systems are retrieved using the detect and spread algorithm and classified according to their top temperatures. Their spatial extension spans a continuous spectrum of individual clouds ranging from 500 km² to 10⁶ km². The spatial distribution of these convective clouds over the Indian Ocean exhibits an increase in convective activity during boreal winter compared to summer. Despite the drastic modification of the synoptic environment over the seasonal cycle, intrinsic cloud properties in January and July are shown to be very similar.

The intrinsic cloud properties that are retrieved are the convective core area relative to the total cloud area, the area colder than 240 K (corresponding roughly to stratiform precipitation), the average cloud-top temperature of the entire cloud (core and anvil), and the minimum cloud-top temperature within a cloud that is assumed to denote the temperature of the overshooting cloud tops.

The analysis reveals a critical scale of about 10⁴ km², which distinguishes two separate convective regimes of scale-dependent cloud properties. Below the critical scale, the cloud mean effective temperature increases with cloud size and the relative core area decreases with the size. The overshooting cloud-top temperature is invariant to the cloud scale. For scales larger than the critical value, the scale dependence is reversed: the mean cloud temperature decreases, the fractional core area increases, and the overshooting cloud top strongly decreases as the cloud size increases. Essentially, the area of undiluted deep convective core increases with the total area of the cloud system, in turn affecting the macroscale properties such as cloud greenhouse effect and tropopause temperature, to name a few. In particular, it is the larger-scale (>10⁴ km²) organized system that penetrates to the tropopause and determines the tropopause altitude, while the smaller scales (<10⁴ km²) hardly reach the upper troposphere. Diurnal variations of the convective cloud cover are also presented with respect to the cloud size. The diurnal cycle of these systems depends significantly on their scale and exhibits complex patterns.

A discussion of these cloud statistics is then offered in the context of general circulation model parameterization.

1. Introduction

Convection plays a central role in the tropical hydrological cycle, basically linking the lower levels of the atmosphere to the upper ones, through water vapor, heat, and momentum transports, feeding the ascending branches of the large-scale circulation. Its associated

cloudiness was suggested as an important factor in the energetic of the Tropics (Ramanathan and Collins 1991). Despite an intensive research effort over the last two decades, on both the observation and modeling fronts, the representation of convection in general circulation models (GCMs) is still not free of problems (Emanuel 1997).

Satellite-based studies of tropical convective cloudiness are widely used to provide validation for GCM behavior (e.g., Morcrette 1991; Weare et al. 1996). However, in-depth validation or guidance for new developments of parameterizations requires more than an estimation of cloud cover. The cloud population forming the ITCZ has long been recognized to encompass a wide variety of convection scale (Sadler 1975; Sikka and Gadgil 1980). The organized convection in tropical mesoscale convective systems is usually considered to span scales from 10 km (the cumulus convection), to 100 km

* Center for Cloud, Chemistry and Climate Publication 206 and INDOEX Report 23.

[†] Current affiliation: Laboratoire de Météorologie Dynamique du CNRS, Palaiseau, France.

Corresponding author address: Dr. Remy Roca, Laboratoire de Meteorologie Dynamique du CNRS, Ecole Polytechnique, 91128 Palaiseau, France.
E-mail: roca@lmd.polytechnique.fr

(the cloud cluster), to 1000 km (the stratiform region; Houze 1993). We consider organized convective systems to have areas of about 10^4 km² or larger. For want of a better phrase, in what follows, we will refer to smaller scales as disorganized convection, usually associated with smaller-scale flow perturbation and/or weak low-level convergence. As shown in Boer and Ramanathan (1997), cloud cover, cloud radiative properties, and lifetime are a strong function of the scale of the clouds for the convective regime of the western tropical Pacific. The treatment of this hierarchy of scale is a challenge for GCM parameterization (Moncrieff and Klinker 1997).

In this study, we document the structural and radiative characteristics of deep convective systems over the Indian Ocean, focusing on their scale-dependent properties in order to highlight the organization of convection over different scales. In particular, we are interested in the differences, if any, between organized convective systems and disorganized convection. Indeed, the Indian Ocean offers an interesting framework for studying the tropical convection, undergoing drastically different patterns over the seasonal cycle. Convective cloudiness forms a well shaped Intertropical Convergence Zone (ITCZ) over the ocean during the early winter monsoon months (Krishnamurti et al. 1997) and different oceanic convection forms as the ITCZ shifts northward to the Indian subcontinent during the summer.

We distinguish between three classes of convective clouds: very deep convection that penetrates to the tropopause (class I), deep convection with cloud tops in the upper troposphere (class II), and deep convective cloud debris (class III). We examine separately the properties of the convective clouds systems, their convective core, and their cirriform anvil. Our motivation is to understand the structure of these systems and provide sufficient data to test convection parameterization theories that account for spectrum of individual clouds (e.g., Arakawa and Schubert 1974).

The first section of the paper introduces the dataset and the methodology we followed. In section 3, the parameters that are representative of the general features of the convective clouds are presented with emphasis on the winter monsoon. Section 4 details the diurnal cycle of the systems. A summary of the findings, as well as a discussion in relation to GCM parameterization and perspectives for future work are proposed in sections 5 and 6.

2. Data and methodology

a. The Indian National Satellite (INSAT) data

The *INSAT-1B* platform is the second geostationary satellite of a first series of multipurpose (telecommunication, broadcasting, and atmosphere imaging) Indian satellites. The Very High Resolution Radiometer images

the earth in two narrow spectral windows: 0.55–0.75 μm in the solar spectrum and 10.5–12.5 μm in the infrared, in about 30 min, every 3 h. The raw numerical counts from the infrared channel are converted into brightness temperature through a lookup table where the resolution is about 0.15 K in the 284–301 K range and 1 K elsewhere (Smith and Mehta 1990). The original spatial resolution of the image is, under nadir conditions, 2.75 km in the solar channel and 11 km in the infrared channel.

The data we use in this study consists of *INSAT-1B* infrared imagery subsampled at the rate of one pixel for every 22 km (one pixel in each direction is kept from the original image) over the period July 1988 and January 1989. These data are archived at the National Center for Atmospheric Research (NCAR). Eight full-disk images were available per day, starting at 0000 UTC. The images were carefully inspected de visu and poor quality images (bad scan lines, missing part of the image) were rejected from the study. The study area covers the oceanic region in the 30°S–30°N, 30°–100°E zone, including the Arabian Sea, the Bay of Bengal, and the open Indian Ocean.

b. The detect and spread algorithm

Single convective clouds are retrieved from the satellite infrared brightness temperature images using the detect and spread (DAS) algorithm (Boer and Ramanathan 1997). This algorithm is a multistage, multithreshold method to delineate individual clouds in the image. It can be seen as a generalization of the clustering approach (Mapes and Houze 1993; Machado et al. 1992). Once the core of cloud is formed by connected pixels colder than a value (the detect stage), then the cloud boundaries are expanded (the spread stage) in all directions until the edges of the cloud (clear sky, another cloud) are encountered.

We use here a variant of the original approach focusing on the retrieval of high clouds only. We limit the warmest brightness temperature associated with an individual convective cloud to 255 K. This limits the edges of the clouds during the spreading stage to stop when clear sky or another cloud or the 255 K value is reached. This threshold was chosen as an upper limit of the cloud temperature generally associated with convection (Mapes and Houze 1993). It is close to the value used over the Atlantic Ocean and Africa (253 K in Machado et al. 1992) or over the Indian Ocean (260 K in Kulkarni et al. 1997). Cloud cores are detected in multiple steps at 220, 235, and 255 K and respectively spread to 240, 255, and 255 K. The overlap between the spread stage and the last detect thresholds prevents new clouds from growing at the edges of an existing one and allows the growth of the boundaries of a detected cloud from a previous step, down to clear sky, or to 255 K, or to an already expanded cloud. On the one hand, the use of the 255 K threshold precludes the

TABLE 1. Cloud classification.

Class	Cloud-top temperature	Comments
Class I	$T_{\text{top}} \leq 220 \text{ K}$	Very deep convection
Class II	$220 \text{ K} < T_{\text{top}} \leq 235 \text{ K}$	Deep convection
Class III	$235 \text{ K} < T_{\text{top}} \leq 255 \text{ K}$	Background convective Cloudiness

inclusion of very thin semitransparent cirrus (which are difficult to differentiate accurately from low-level clouds using the IR channel only) to the cloud and, on the other hand, it prevents the aggregation of low- and midlevel clouds to the convective system. An extended discussion concerning this approach can be found in Boer and Ramanathan (1997, appendix 1).

The parameters that are derived from this processing encompass the longitude, latitude, and local time of the centroid of the cloud; its total area; its minimum and averaged brightness temperature, as well as the area below 220 and 240 K within a cloud.

c. Convective cloud classification

The coldest temperature reached within a cloud, referred to here as the *overshooting cloud-top temperature*, is used to segregate the convective clouds. Three classes are formed according to the rationale provided in Table 1. The first class encompasses cloud-top temperatures colder than 220 K. These *very deep convective* systems contain at least one pixel colder or equal to 220 K, a threshold delineating the core of the convective systems (Laing and Fritsch 1993). By setting such a criterion, the coldest temperature in this class is bounded on the warm side (at 220 K) but free on the cold side and hence can reach up to the highest levels of the troposphere [see section 3c(3) for a discussion].

The class II population has its cloud-top temperatures between 220 and 235 K and is referred to as the *deep convective clouds* and corresponds to either deep convection found in the vicinity of the large class I clusters or isolated convective events reaching the mid- to upper troposphere. The third class contains clouds with their tops warmer than 235 K and implicitly colder than 255 K. This last class, the *background convective cloudiness*, might as well include some tops of midlevel cloud systems, isolated thick cirrus, or detached stratiform anvils of decaying convective clouds, and can be thought as the so-called *convection debris* that is often encountered during the winter monsoon over the Indian Ocean region (Webster and Stephens 1980; Krishnamurti et al. 1997). Figure 1 shows the combined effect of the DAS algorithm and of the above-mentioned classification for an image taken on 1 January 1989 at 0000 UTC over a limited part of the study area. The original image (Fig. 1a) exhibits classic features of convective cloudiness over the tropical ocean that forms the ITCZ, namely, organized large-scale clusters spanning different IR temperatures. Some warmer pixels are also encountered

over homogeneous areas, for instance, over the south-east part of the image, likely low-level clouds. The very deep convective clouds are presented in Fig. 1b. The central systems, for instance, have been successfully extracted, and the feature in the eastern part of the original image has been split in many different individual systems. On the western part of the image, two very deep convective systems have been detected with connected ends. A merging process of these two convective clouds is indeed under way as revealed by an inspection of the next time step image (not shown).

The second class offers the same kind of characteristics, exhibiting isolated as well as tightly close cells. Note that in this particular image the spatial scales associated with the deep convective clouds are smaller than the class I main scales. In the central-east part of the image, several clouds are found in the vicinity of the previously detected class I systems and correspond to smaller and less deep convection associated with this system (Houze and Betts 1981). Similarly, the convection debris clouds are detected around the convective cores of previously detected clouds as well as isolated features away from the main convective area, and their main scales are smaller than the previous two classes of clouds.

This classification in terms of cloud height allows us to document the full spectrum of convective clouds and offers a relevant characterization of these systems along the lines of the Arakawa and Schubert parameterization scheme (Arakawa and Schubert 1974) that is currently used and updated in GCMs (Cheng and Arakawa 1997; Randall et al. 1997).

3. Properties of convective cloudiness over the Indian Ocean

In the following sections, results are presented for both July 1988 and January 1989 as representative of the summer southwest and winter northeast monsoons synoptic activity over the study area. For convenience, typical resolution of spectral GCMs have been overlaid on the figures. Only clouds that have at least 50% of their area over the ocean are used in these statistics, that is, in coastal regions clouds with more the 50% of their extend over land are excluded.

a. Spatial distribution

Figure 2 shows the monthly mean cloud cover associated with the three different classes of convective clouds for January and July. The spatial cloud cover is computed over a $2^\circ \times 2^\circ$ grid, as the ratio of the of the cloud extent to the observed area. When clouds overlap different grid points or spread over several grid points, the cloud cover is accordingly distributed over these points. The January features encompass a well-formed ITCZ with peaks of very deep convective cloud cover southwest of Borneo, as well as northwest of Mada-

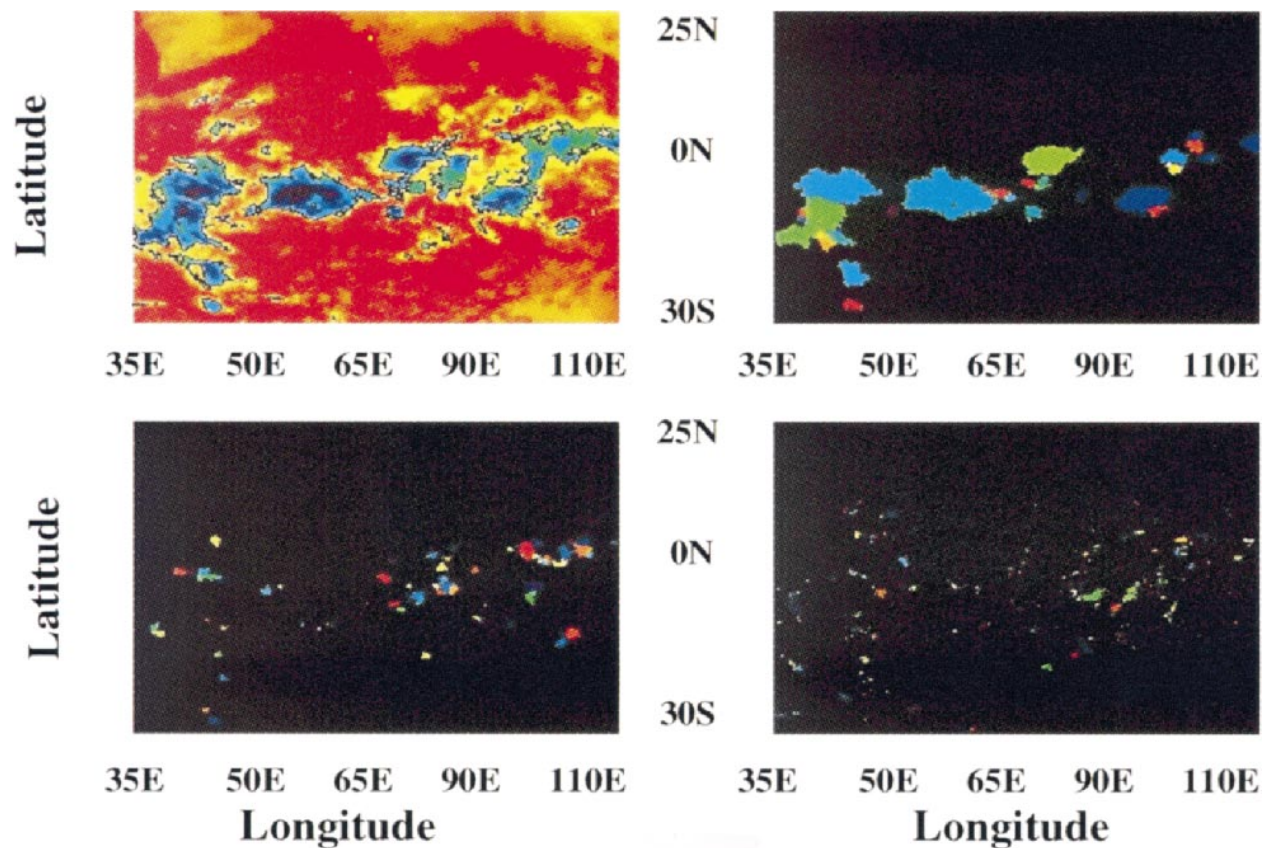


FIG. 1. Segmentation of the original image. (a) Original INSAT-1B image for 1 Jan 1989 at 0000 UTC, with the 255 K isotherm overlaid, (b) class I, (c) class II, and (d) class III. A random color is attributed to each individual cloud.

gascar and an overall relatively strong convective activity over the ocean. The two other cloud classes exhibit smaller contribution and more homogeneous distributions of their associated cloudiness. Recall that the retrieved clouds are restricted to oceanic regions.

The summer convective cloud seems to surround the Indian subcontinent with a strong contribution from class I clouds, with a local maximum of 30% in the Bay of Bengal. A high concentration of all three of the classes of clouds is found in the eastern Arabian Sea, associated with the monsoon clouds that form over the ocean before landing on the subcontinent. A secondary zone of convection is nevertheless located over the Indian Ocean around 5°S with local cloud cover larger than 20%.

The major synoptic differences between the two monsoonal regimes are as follows.

- The class I very deep convective clouds are more prevalent during the winter monsoon than the other type of convective clouds.
- Winter monsoon deep convection extends over the entire Indian Ocean, from Africa to Indonesia, predominantly in the Southern Hemisphere with a secondary maximum just north of the equator, while during the southwest monsoon, the area of convection is

restricted to the eastern part of the Indian Ocean (east of 60°E).

- Deep convective clouds extend into the Bay of Bengal only during the southwest monsoon.

The INSAT dataset available at NCAR also encompasses images from the 1985–88 period at a lower diurnal sampling rate (two images per day instead of the eight images per day presently used for July 1988 and January 1989). A quick look at these data extends the above findings to the other years. However, a modulation of the convective activity is found at the interannual scale when compared to July 1988 and January 1989. These latter months indeed corresponds to a cold phase of the El Niño–Southern Oscillation and positive rainfall anomalies were observed over the Indian Ocean during this period (Janowiak and Arkin 1991). As suggested by Gray et al. (1992), the deep convection intensity over this region of the world's ocean might be modulated at the interannual scale by the interactions of the phase of the quasi-biennial oscillation with El Niño/La Niña events. A detailed analysis of the interannual variability of convection over the Indian Ocean and of the underlying mechanisms responsible for these variations is out of the scope of the paper but it is a topic for future research.

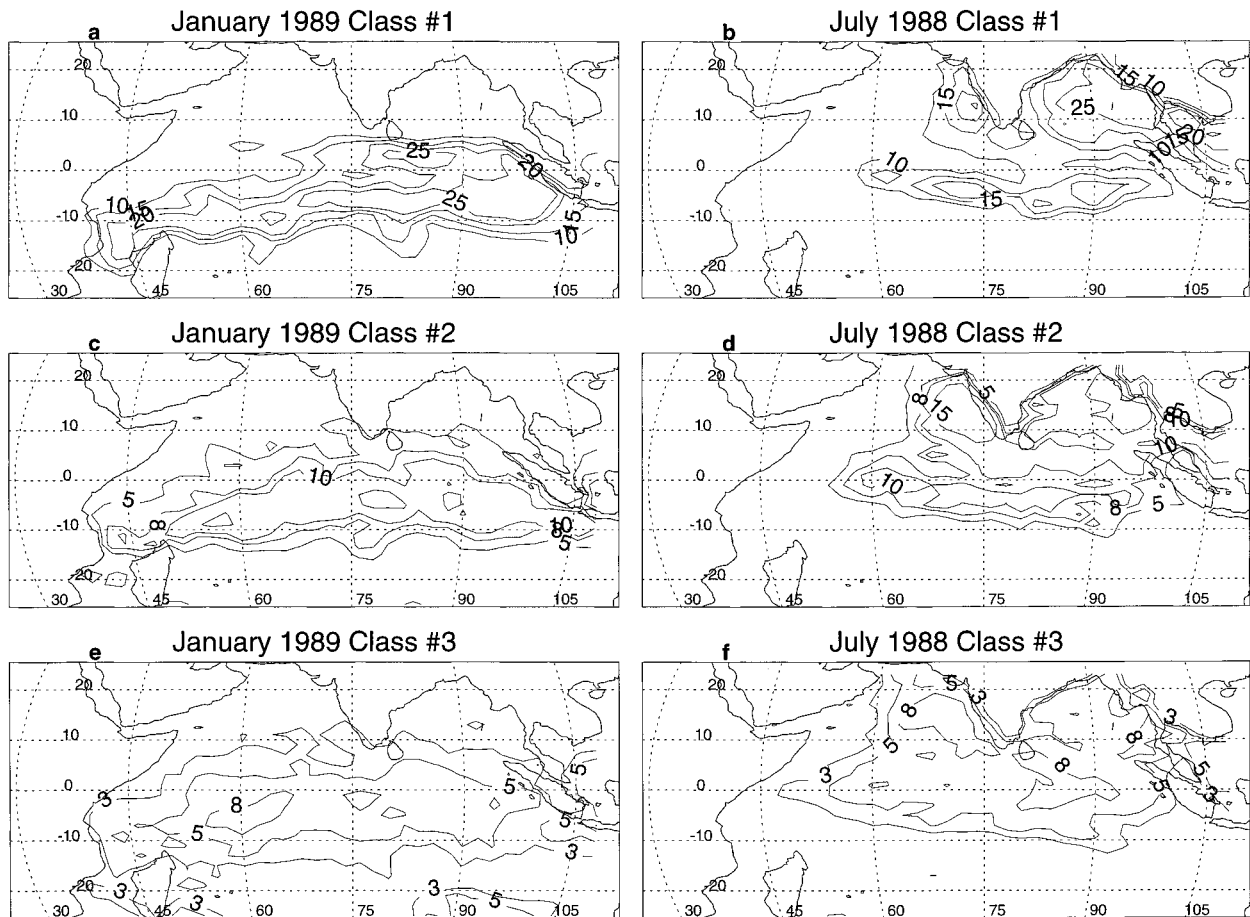


FIG. 2. Spatial distribution of convective cloud cover. The left panels correspond to Jan 1989 and the right panels to Jul 1988 for the three cloud classes. The value of the isolines are indicated on the figure and are different for each class.

b. Scale dependence of convective cloud cover

The top two panels of Fig. 3 show the number distribution of clouds binned according to their size. The frequency was computed by normalizing the total number of clouds in each bin by the number of available images in the month.

Both January and July reveal similar patterns. The class I and II number distribution peak around an area of 10^4 km² while class III increases toward smaller sizes. The maximum area of in all of the three classes can reach sizes as large as 10^6 km². Around 10^6 km², there is an order of magnitude more class I very deep convective clouds than the other classes. In terms of these latter clouds, a GCM with a resolution of T213 (about 50×50 km grid size at the equator) should be able to resolve most of them (95%) without an explicit parameterization. It should be noted, however, that the GCM would need a convection parameterization to treat the momentum and mass fluxes.

The cumulative area is shown in the bottom two panels. Class I contributes most to the total area for both January and July. For all three classes, clouds

with areas between 5000 km² and 10^6 km² contribute more than 95% to the total convective cloud area. Thus a GCM with a T213 (50×50 km) resolution should be able to resolve most of the radiatively active convective clouds, while a T42 (250×250 km) or T21 (500×500 km), used in most global warming studies (Intergovernmental Panel on Climate Change 1995) will need to parameterize most of these cloud systems.

c. Structural characteristics of the convective systems

In what follows, we explore a cloud size spectrum ranging from 500 km² to 10^6 km², that is, from isolated small convective clouds up to highly organized convective systems. The smallest scales (below around 10^4 km²) are associated with spatially *disorganized* (or random) convection and the larger scale (over about 10^4 km²) with *organized* convection that includes meso-scale convective systems and tropical storms (e.g., Shemo and Evans 1996).

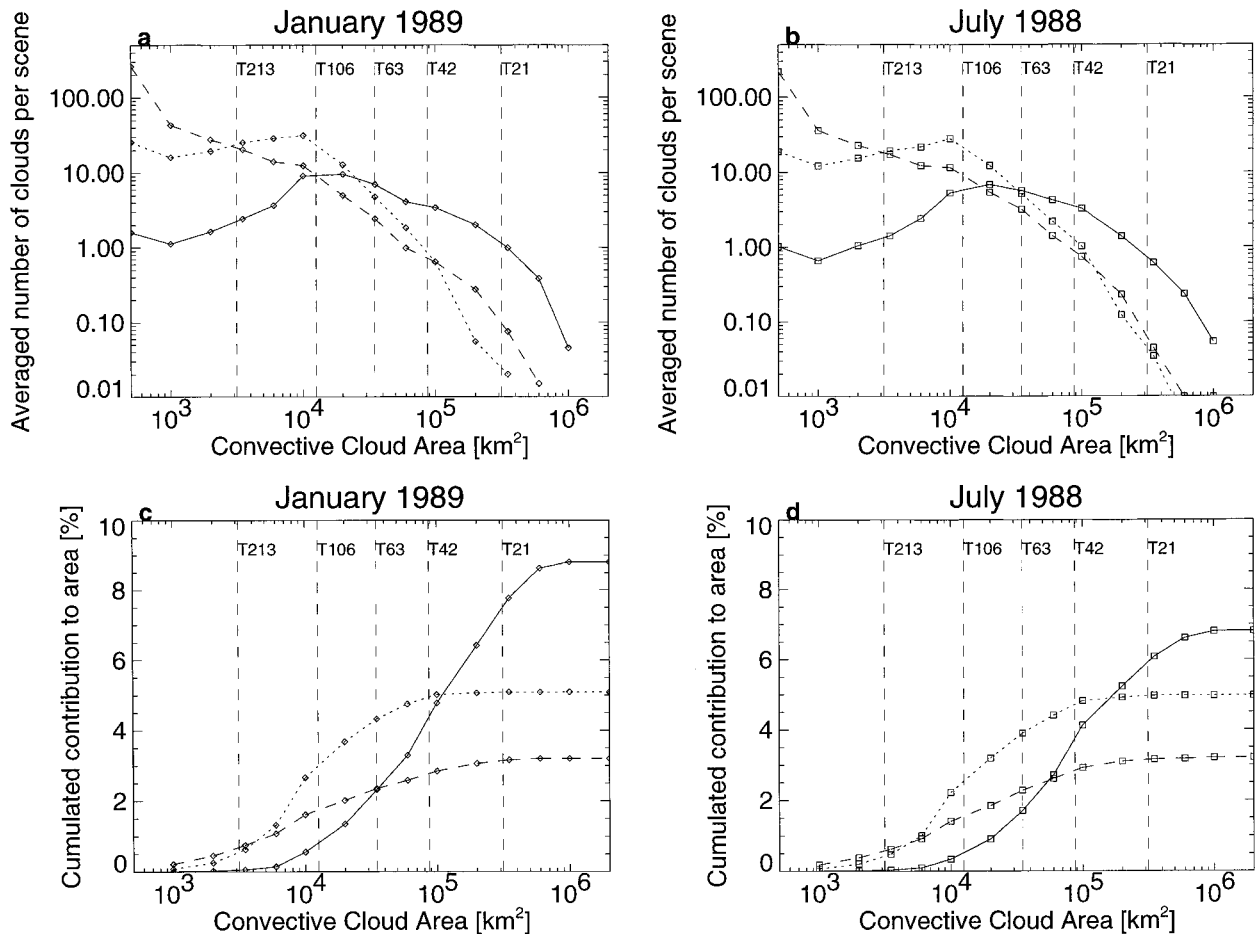


FIG. 3. Convective systems occurrence (upper panels) and cumulated cloud cover in percent (%) (lower panels). Plain lines correspond to class I, dotted to class II, and dashed to class III. Jan 1989 (left) and Jul 1988 (right). Typical GCM resolution has been overlaid.

The conceptual model of the large cloud clusters associated with tropical convection that we follow is that summarized in Houze and Betts (1981), which consists of the following: a cumulus core formed of embedded single convective cells where heavy rain rates take place and a stratiform anvil composed of high cloudiness ranging from thick to thin cirrus clouds.

In this section, we investigate the cloud-type partitioning of the convective clouds and its dependence upon the cloud scale, with emphasis on the core of the class I systems.

1) AVERAGE CLOUD TEMPERATURE

For optically thick clouds, the cloud greenhouse effect (or the longwave cloud forcing) is a linear function of the difference between the surface temperature and the cloud-top temperature (Ramanathan 1977). In our case, the sea surface temperature over which cloud forms does not depart much from 300 K, hence the leading parameter that determines the cloud greenhouse effect is the cloud-top temperature.

Figure 4 shows the average (over the full cloud, including the core and the anvil) cloud-top temperature as a function of the cloud size. We first note that the two seasons reveal very similar patterns. The class II and III clouds show little dependence of their average temperature upon the scale. However, very deep class I convective clouds exhibit a strong scale dependence: the smallest and largest scales have very low brightness temperature, while the medium-sized clouds (around 10⁴ km²) have the warmest average cloud-top effective temperature.

Assuming clouds to be black and variations of the SST to be small, the cloud greenhouse effect increases linearly by about 1.65 W m⁻² per each degree drop in the cloud-top temperature (Ramanathan 1977), and increases linearly with cloud cover. As a result, the decrease of cloud-top temperature with cloud size clearly confers an overwhelming role of the larger organized cloud systems to the cloud longwave forcing over the Indian Ocean.

We investigate next the distribution of effective temperature within a cloud responsible for these mean values.

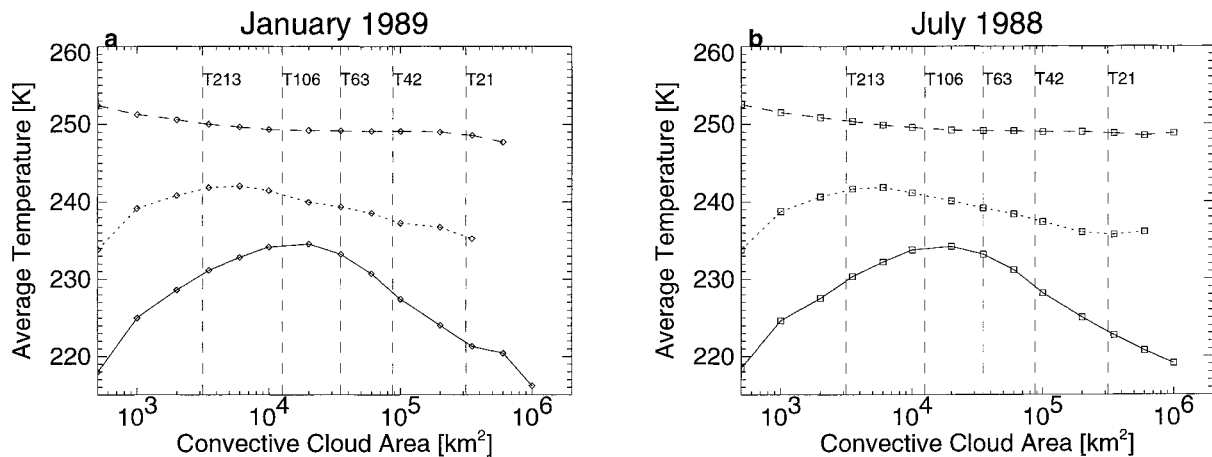


FIG. 4. Cloud average brightness temperature function of the cloud size for (a) Jan and (b) Jul. Plain lines correspond to class I, dotted to class II, and dashed to class III. Typical GCM resolution has been overlaid.

2) THE STRATIFORM ANVIL

Convective activity or precipitation is usually related to brightness temperature colder or roughly equal to 240 K at a common geostationary satellite footprint resolution of a few kilometers (e.g., Janowiak and Arkin 1991; Laing and Fritsch 1993). This value is here used as a first-order indicator of the precipitation or convective activity within the cloud (including the convective core at different heights and the stratiform precipitating cloudiness associated with the anvil), as opposed to pixels with warmer than 240 K brightness temperatures, that we consider as an indicator of the nonprecipitating cirrus clouds that constitute the remnant part of the cloud.

Figure 5 shows the 240 K and colder area within a cloud as a function of the cloud size for January (Fig. 5a) and July (Fig. 5b). For the three cloud classes, this area increases monotonically as the total cloud size increases. The overall pattern is very similar in both months. Figures 5c,d show this same variable normalized to the cloud total area function of the cloud size. Class III shows very little dependence of the partitioning upon size, indicating a fairly constant structure of this convective debris with size. Both class II and class I clouds reveal a strong scale dependence. Class II clouds from 500 km^2 up to around $6 \times 10^3 \text{ km}^2$ reveal a decrease of their fractional precipitation area as the cloud size increases, whereas for the larger scale the trends are reversed. Very deep class I clouds behave like class II with a shift of the reversal scale to around $2 \times 10^4 \text{ km}^2$.

Despite a clear increase of the absolute 240 K and colder area over the entire size spectrum, it appears that there is a degree of spatial organization of convection, over and below which the structure of the clouds dependence upon the cloud scale differs drastically.

The nonprecipitating cirriform part of the anvil (the area warmer than 240 K) can be as large as 60% (30%)

for the class II (class I) clouds. The largest and coldest systems of class I reach up to a million square kilometers with only 15% of their total area composed of nonprecipitating cirrus clouds. It should be recalled that the cloud retrieval algorithm is, here, limited to temperature colder than 255 K precluding from adding the warmer (and thinner) cirrus to the system. The above estimations should hence be regarded as underestimates of the nonprecipitating cirrus fraction of the clouds. The potential important effect on the radiation budget of these cirrus clouds effect, is nevertheless, an important factor that must be incorporated into GCMs.

3) PROPERTIES OF THE CONVECTIVE CORE

The next important component of convective systems is the so-called convective core where most of the convective updraft and precipitation occurs. The convective outflow, which provides moisture for the cirrus to grow, also emanates from this region.

According to our classification, class I very deep convective clouds encompass effective temperature colder than the usually considered 220 K value for delineating the convective core of tropical clouds cluster. Figure 6a shows the core area as a function of the cloud size. The convective core area monotonically increases as the cloud size increases. However, when normalized by the total cloud area, the fractional area of the core peaks for the smallest and largest clouds and is minimum in between, above 10^4 km^2 (Fig. 6b). The degree of spatial organization of convection over which trends are reversed corresponds well with the 100-km scale around which a mesoscale circulation take place within the systems (Redelsperger 1997; Houze 1993). Within the several tightly embedded single cells or "hot towers" that form the convective core of the cloud, we now focus on the deepest one by estimating the coldest temperature within a cloud. These overshooting cloud-top temper-

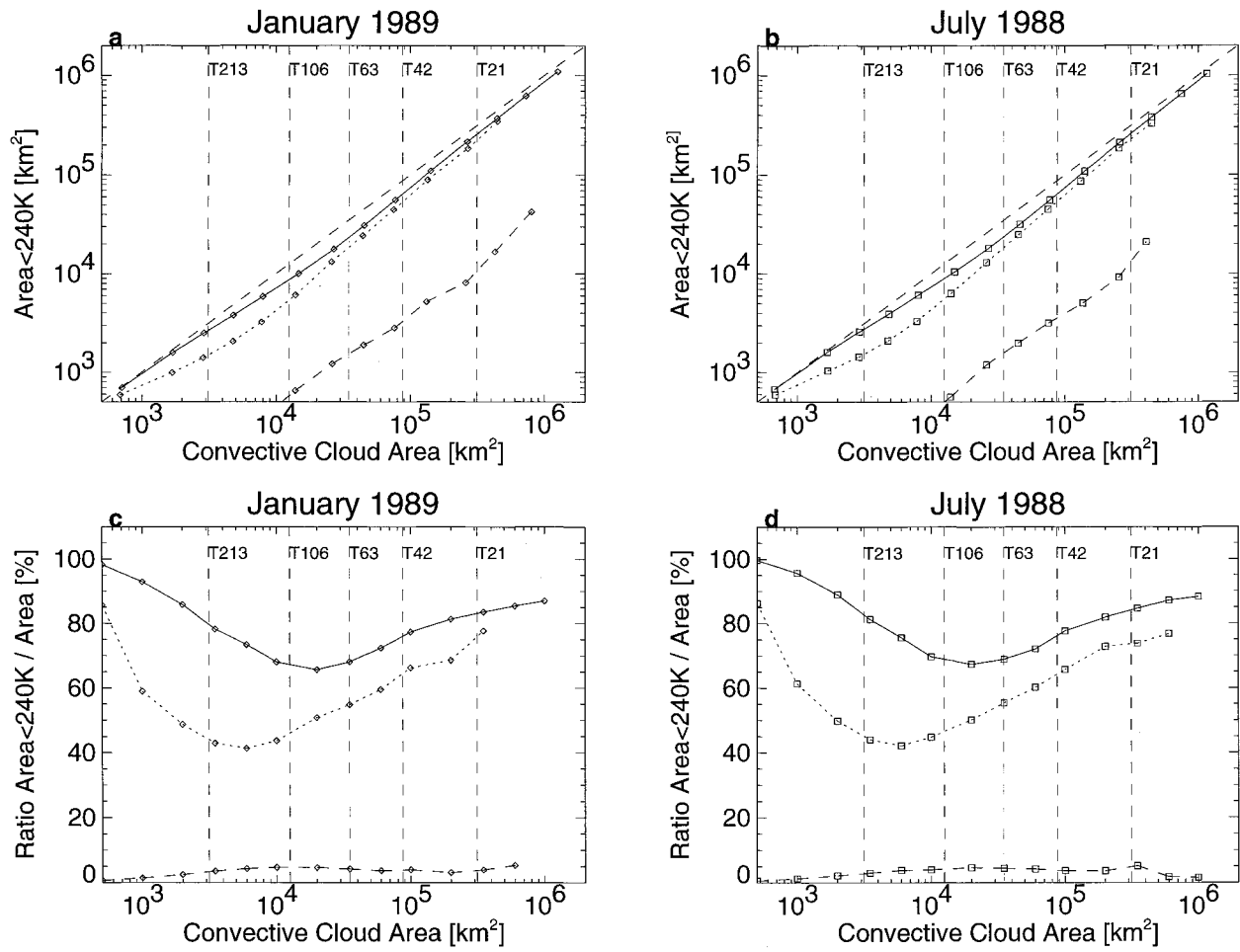


FIG. 5. Precipitating part of the convective systems. (top) Absolute (km²) and (bottom) relative to the total system (%) area of the convective systems for (left) Jan and (right) Jul. Plain lines correspond to class I, dotted to class II, and dashed to class III. Typical GCM resolution has been overlaid.

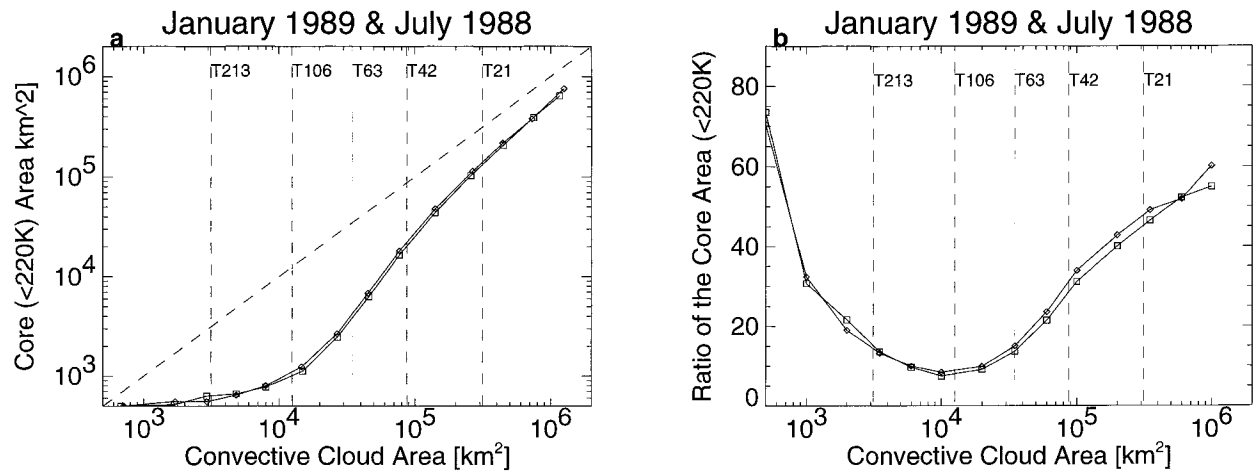


FIG. 6. Core of the very deep convective cloud systems. (a) Absolute (km²) and (b) relative to the total system (%) area of the convective core. Jan (♦) and Jul (□).

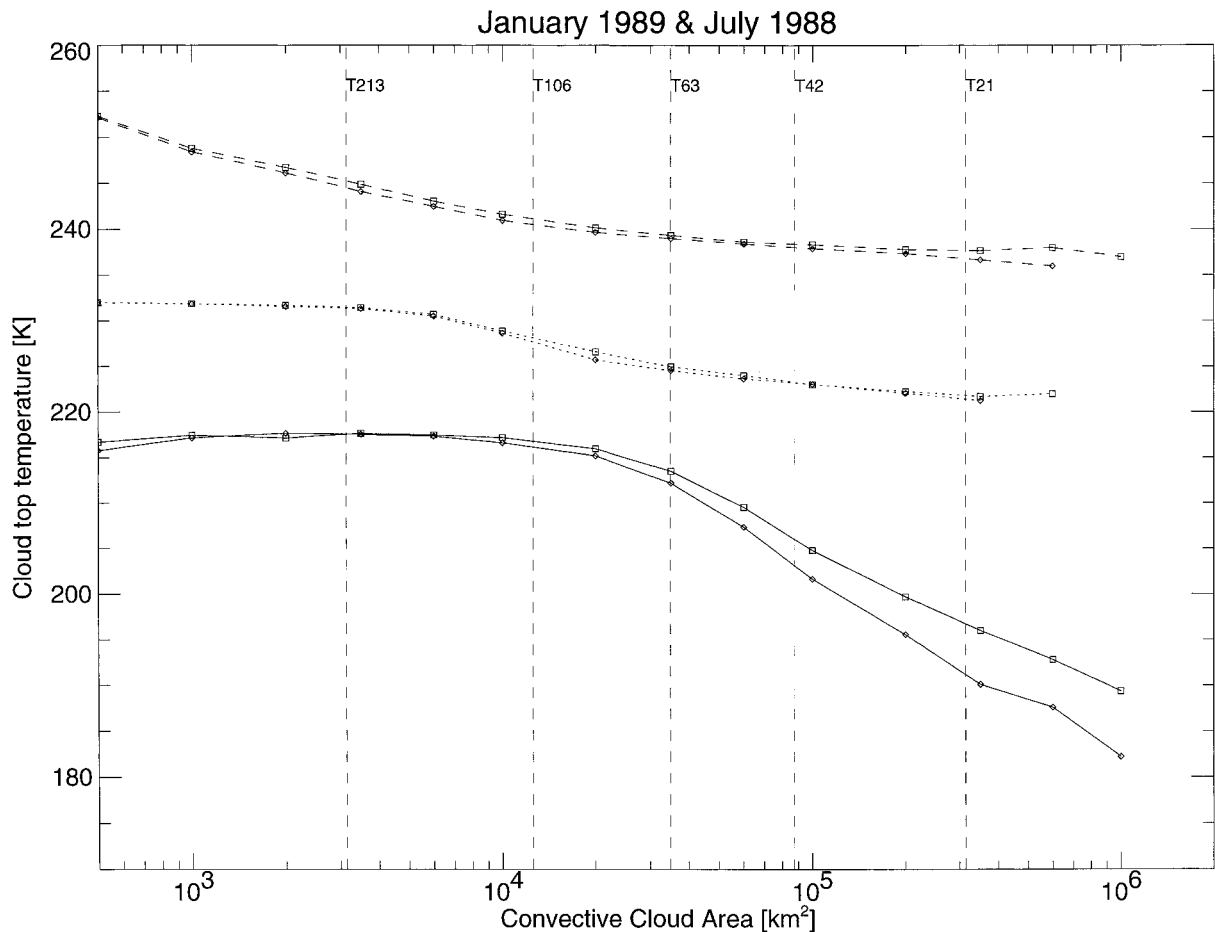


FIG. 7. Cloud overshooting top temperature function of the cloud size. Jan (\blacklozenge) and Jul (\square). Plain lines correspond to class I, dotted to class II, and dashed to class III. Typical GCM resolution has been overlaid.

atures that we used for the classification are presented, as a function of the cloud size, in Fig. 7. Irrespective of the convective cloud categories, there is a general tendency for the larger cloud to have a deeper cell. This behavior is more pronounced for class I clouds.

The very deep convective clouds (class I) indeed show no cloud size dependence of their deepest convective cells (around 217 K over the 500 km^2 – 10^4 km^2 cloud size range) until the spatial organization of the cloud reaches up to the 1 – $2 \times 10^4 \text{ km}^2$ scale when the overshooting top becomes strongly dependent upon the cloud size, being colder as the cloud size increases.

The above findings have important implications on the role of deep convection in the maintenance of the tropical tropopause. This fundamental relationship between the size of the cloud (or its degree of organization) and the overshooting top temperature of the deepest convective cells in the core of a tropical cloud system over the Indian Ocean, may be explained as follows: the entrainment of unsaturated air from the environment is inhibited when the core is protected by the cloudy region, thus enabling it to reach higher altitudes, as

opposed to isolated cells or small clouds that do not benefit from such protection (Lopez 1978).

An interesting definition of the tropical tropopause is suggested by Highwood and Hoskins [1998] that physically links convection and tropopause temperature. The temperature of the top of the convective heating region (or our overshooting cloud-top temperature) indeed allows a definition of tropopause consistent with simple climate change models where the region above this level can be considered in radiative equilibrium, whereas the so-defined troposphere would be in radiative–convective equilibrium. Figure 7 shows that, for a given season, only the largest systems ($5 \times 10^4 \text{ km}^2$ and larger) reach up to the tropopause like annual mean temperature of around 200 K. The Indian Ocean region is characterized by a marked seasonal cycle of the tropopause temperature: warmer in summer than winter by about 4–5 K (Highwood and Hoskins 1998). This expected seasonal cycle is also revealed in Fig. 7 where the overshooting cloud-top temperature in July, averaged over the 10^5 km^2 and larger clouds, is about 5 K warmer than in January. The tropopause temperature, according to this

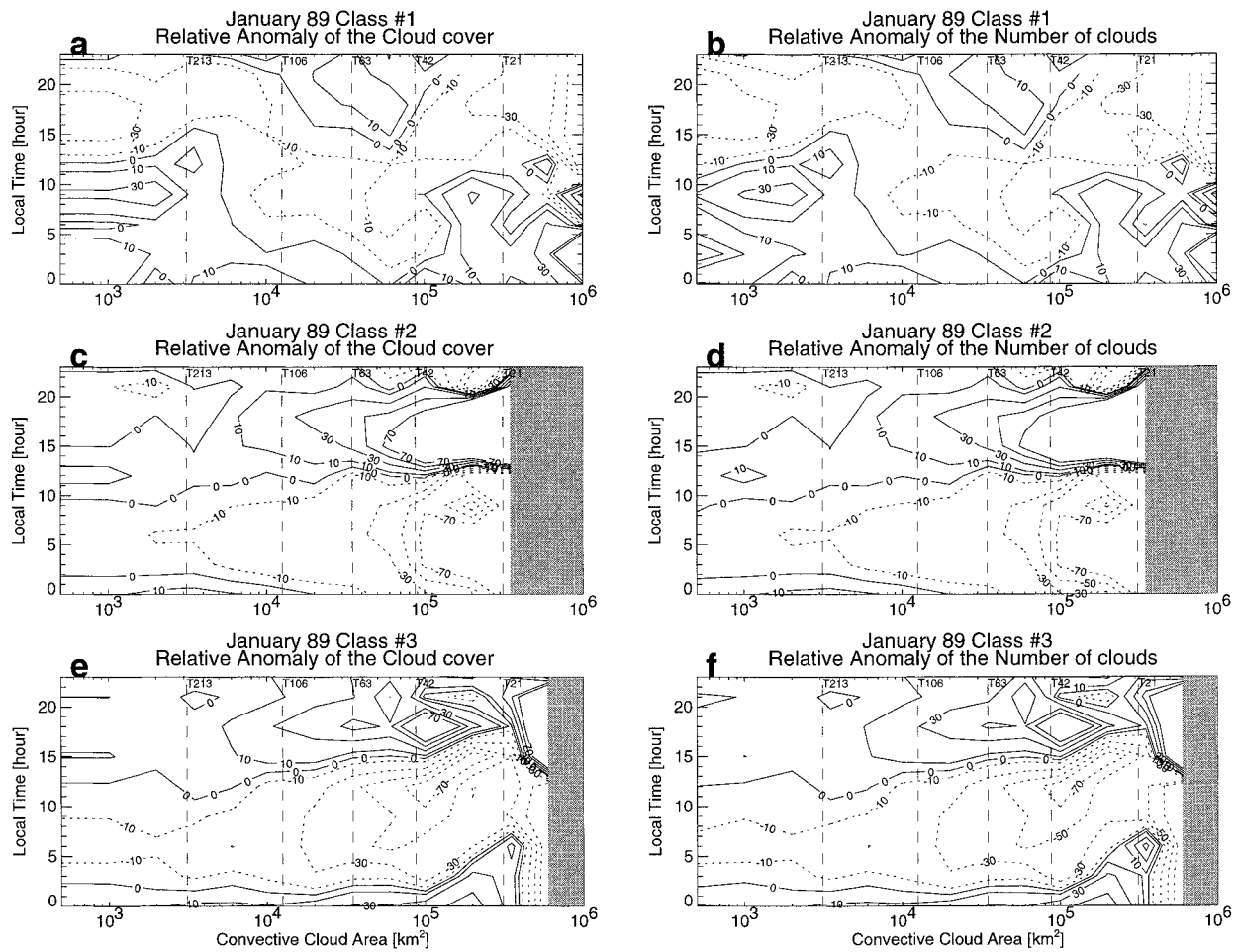


FIG. 8. Diurnal cycle of the convective activity for Jan 1989. The left panels correspond to the anomaly of cloud cover over the diurnal cycle for the three convective cloudiness classes (from top to bottom), in percent. The right panels show the associated anomaly of number of clouds. The time interval is 3 h. Typical GCM resolution has been overlaid. Gray shaded zone indicates that no cloud was found.

definition is hence, mainly driven by the organized convective systems rather than by disorganized systems.

4. Diurnal statistics

The diurnal cycle of oceanic convection shows globally some systematic maximum in the morning around 0600–0900 LST (Hendon and Woodberry 1993) and some regional particularities [e.g., Chen et al. (1996) over the Pacific warm pool; Williams and Houze (1987) over the maritime continent; Desbois et al. (1988) over the eastern Atlantic Ocean]. As shown in section 3, the summer cloudiness distribution will be more sensitive to the Indian subcontinent influence so that we here focus on the winter monsoon as a better representation of open oceanic convection.

The local time associated with each of the clouds is computed according to the UTC observation time of INSAT and the cloud centroid longitude and the statistics have been binned every 3 LST. The cloud cover anomaly along the diurnal cycle is computed for each

local hour and cloud size for the three classes and is expressed in percents relatively to the mean daily cloud cover shown in Fig. 3. This variable sums up to zero over the diurnal cycle for a given size bin. The relative number of clouds per hour bin and size was computed similarly from the occurrence distribution. Figure 8 shows these parameters for each of the three cloud classes. Both the diurnal anomaly of the cloud cover and the relative number of clouds show significant diurnal cycle for the three classes. The class I very deep convective clouds exhibits a strong-scale dependence of the cloud cover diurnal anomaly: (i) the smaller clouds peak around 0900 LST with a positive anomaly from midnight to midday, (ii) the medium clouds (10^4 km² to 10^5 km²) varies slightly from -10 to 10% with a positive anomaly starting in the late afternoon up to midnight, (iii) the larger convective systems peaks during the night and early morning with a negative anomaly from midday to midnight.

Class II and III clouds show almost no scale dependence in the sign of the cloud cover diurnal anomaly.

The zero anomaly isoline for the two classes is between 0900 and 1200 LST for class II and between 1200 and 1500 LST for class III, over the full size range. However, cloud cover anomaly intensity appears to be scale dependent with smaller variation for smaller cloud and large departure from the mean for the largest systems.

A T213 resolution GCM should be able to reproduce the different behavior of the smallest, medium, and largest scale clouds, and the difference between the three classes, whereas a T21 resolution GCM can not account for such scale dependence.

5. Summary

We have developed a procedure for retrieving individual convective systems from the INSAT infrared imagery and apply it over the Indian Ocean for different seasons. The main findings of this study are the following.

- Convective cloud systems form a continuous ensemble of clouds with size ranging from 500 km^2 to 10^6 km^2 .
- Two main regimes of scale-dependent cloud properties characterize this ensemble: regime I or disorganized convection with size below a critical scale of around 10^4 km^2 (T106 GCM resolution) and regime II or organized convection with size larger than 10^4 km^2 .
- The class I very deep convective cloud corresponds to more than 50% of the total convective cloud cover in January (around 50% in July) and is mainly composed of organized convective systems.
- The greenhouse effect of convective cloud (related to their average effective temperature) decreases with the cloud size for the disorganized convection regime and increases with the cloud size for the organized systems. The class III cloud average temperature shows only little scale dependence.
- The overshooting cloud-top temperature shows no dependence on the cloud size for the disorganized convection. For the organized convective systems, it decreases with cloud size, especially for the very deep clouds, suggesting that, the tropopause temperature is mainly driven by the overshooting cloud-top temperature of the class I organized convective systems.
- The diurnal cycle of class I clouds is drastically different from the two other classes. Class I diurnal cycle is a strong function of the cloud size whereas class II and III exhibit only a slight dependence of the diurnal cycle upon the scale.

Furthermore, the cloud intrinsic properties revealed here have a strong similarity between January and July, despite drastic modifications of the synoptic environment from the winter to the summer monsoon. This seasonal invariance enables us to draw some general inferences about parameterization of convective cloud

systems in general circulation models. We discuss these in this section.

6. Implication for convection parameterization in GCM

GCMs generally used for climate simulation have spatial resolution ranging from T21 (roughly $500 \text{ km} \times 500 \text{ km}$ grid box at the equator) to T42 ($250 \text{ km} \times 250 \text{ km}$) while the forecast models have much higher resolution from T106 to T213 ($50 \text{ km} \times 50 \text{ km}$). The observed, scale-dependent cloud properties presented here can be used to constrain the framework of cloud parameterization in GCM.

Indeed, the size distributions (Figs. 3a,b) reveal the relative fraction of parameterized clouds versus the resolvable and resolved ones (we here refer to resolvable clouds as those whose sizes are larger than the grid-box size, and to resolved clouds those whose sizes are twice as large as the grid box). At a T213 resolution, most of the convective clouds of class I and II will be resolved rather than parameterized. The opposite applies to the T21 resolution. The corresponding cloud cover (Figs. 3c,d) implies that, at a T213 resolution, almost all of the class I cloud cover will be due to resolvable or resolved clouds (90% for class II and 85% for class III). However, most of the GCMs used for climate and global warming studies have grid resolutions larger 10^5 km^2 , and such GCMs have to parameterize a large fraction of the convective cloud systems.

The diurnal statistics presented in section 5 may be used as a rigorous test of the convective parameterization and large-scale flow interactions since the diurnal behavior of the model convective clouds cannot be tuned. For instance, in a T21 resolution model, clouds will peak from midnight to early morning, whereas a finer grid should allow a more detailed description of the scale dependence of the diurnal cycle shown in Fig. 8.

The cloud spectrum here depicted over the Indian Ocean encompasses a wide range of cloud overshooting temperature and associated size. The smaller size range of cloud ensemble population is reaching up to the mid-to upper troposphere, whereas the tropopause levels are attained only by the convective cells embedded in the large cloud clusters. The implementation of a convection parameterization based on such individual cloud ensemble should hence limit the detraining top level according to the degree of organization of convection and unique detraining levels at the tropopause should be avoided.

The sensitivity of the quality of the model simulation of convection to the vertical resolution is known to be a major issue. To put it in perspective, consider a standard tropical atmosphere and its upper-tropospheric ($250\text{--}100 \text{ mb}$) lapse rate of 6.5 K km^{-1} and assume a GCM with a vertical resolution of about 2 km in the upper troposphere. The resulting uncertainty of the tem-

perature in the vertical would be about ± 6.5 K. The properties of the regime II clouds would be strongly influenced.

As an example, let us consider the radiative properties of an individual black cloud system of class I. Assume the cloud size to be 6×10^4 km² and a T21 resolution grid box (the cloud cover is 0.2). Its average temperature is about 231 K (Fig. 4). Consider a typical tropical SST of 300 K and let us note $F = c_1 - c_2 \times A_c$, the outgoing longwave radiation (OLR), with c_1 being the clear-sky OLR at the top of atmosphere, c_2 being the cloud effect, and A_c the fractional cloud cover (A_c also depends on the cloud temperature as in Fig. 4). Further, c_2 is equal to $1.65 \text{ W m}^{-2} \text{ K}^{-1}$ (Ramanathan 1977). The OLR hence depends on both, the surface temperature T_s , and the cloud temperature T_c . We shall hold the SST fixed in order to isolate the effect of the cloud-top temperature uncertainty on the OLR. The uncertainty in the OLR due only to the uncertainty in the cloud-top temperature (i.e., neglecting any cloud size–cloud-top temperature relationship) is simply equal to $\pm 2 \text{ W m}^{-2}$. Figure 4 indicates that an uncertainty of 6.5 K in the cloud-top temperature is associated with a factor of about 3 of uncertainty in the cloud size. The uncertainty in the OLR, including both the temperature and the size effect, is now equal to -52 W m^{-2} for the colder (and bigger) extreme of a -6.5 K error and around $+16 \text{ W m}^{-2}$ on the warmer (and smaller) extreme. This simplistic calculation stresses the importance of the cloud size–cloud temperature relationship on the radiation budget.

The dynamical processes of deep convection leading to the extensive cloud shields take place at very small scale (10 km). The scale that separates the regime of organized and disorganized convection appear to take place around 10^4 km², corresponding roughly to a T106 resolution. Moncrieff and Klinker (1997) investigated a case study of a large cloud cluster simulation in the Pacific warm pool using the European Centre for Medium-Range Weather Forecast model. They showed that the T213 resolution of the model and the simultaneous use of an elaborated mass flux scheme for convection parameterization results in a cloud that is partly resolved and partly parameterized, leading to erroneous momentum transport and interactions with the large-scale flow. They furthermore suspected this spurious effect to occur between T106 and T213 resolutions, closely related to our T106 critical scale for the Indian Ocean.

The fundamental convective cloud properties presented here (cloud greenhouse effect, detrainment level of moisture by convection, intracloud rainfall, and deep convection activity distributions) are all but central to the global warming theory, and parameterizing this multiscale dynamical processes and associated cloud cover in a high-resolution GCM is an important challenge. A promising venue to tackle these multiscale issues may lie in the delocalized physics approach (Vintzileos and Sadourny 1997) where parameterizations and dynamics can be run on different grids in the same GCM. The

data presented here will be particularly important for such scale-dependent approaches.

Acknowledgments. The authors acknowledge the National Center for Atmospheric Research and the India Meteorological Department for making these data available. Dr. Boer's insights into the detect and spread algorithm are very appreciated. We thank the two anonymous reviewers for their helpful comments. This study was performed when the first author was a Coopérant du Service National Français at C4 detached by the French Ministry of Defense to the French Ministry of Foreign Affairs and the French Ministry of Cooperation. This study was funded by the National Science Foundation (Grant ATM-9405024) and the Department of Energy (Grant DEFG-0391-ER61198).

REFERENCES

- Arakawa, A., and W. H. Schubert, 1974: Interaction of a cumulus cloud ensemble with the large-scale environment, Part 1. *J. Atmos. Sci.*, **31**, 674–701.
- Boer, E. R., and V. Ramanathan, 1997: Lagrangian approach for deriving cloud characteristics from satellite observations and its implications to cloud parameterization. *J. Geophys. Res.*, **102** (D17), 21 383–21 399.
- Chen, S. S., R. A. Houze Jr., and B. E. Mapes, 1996: Multiscale variability of deep convection in relation to large-scale circulation in TOGA COARE. *J. Atmos. Sci.*, **53**, 1380–1409.
- Cheng, M. D., and A. Arakawa, 1997: Inclusion of rainwater budget and convective downdrafts in the Arakawa–Schubert cumulus parameterization. *J. Atmos. Sci.*, **54**, 1359–1378.
- Desbois, M., T. Kayiranga, B. Gnamien, S. Guessous, and L. Picon, 1988: Characterization of some elements of the Sahelian climate and their interannual variations for July 1983, 1984, and 1985 from the analysis of METEOSAT ISCCP data. *J. Climate*, **1**, 867–904.
- Emanuel, K., 1997: Overview of atmospheric convection. *The Physics and Parameterization of Moist Atmospheric Convection*, R. K. Smith, Ed., Kluwer Academic Publishers, 1–28.
- Gray, W. M., J. D. Sheaffer, and J. A. Knaff, 1992: Hypothesized mechanism for stratospheric QBO influence on ENSO variability. *Geophys. Res. Lett.*, **19**, 107–110.
- Hendon, H. H., and K. Woodberry, 1993: The diurnal cycle of tropical convection. *J. Geophys. Res.*, **98** (D9), 16 623–16 637.
- Highwood, E. J., and B. J. Hoskins, 1998: The tropical tropopause. *Quart. J. Roy. Meteor. Soc.*, **124**, 1579–1604.
- Houze, R. A., Jr., 1993: *Clouds Dynamics*. International Geophysical Series, Vol. 53, Academic Press, 570 pp.
- , and A. K. Betts, 1981: Convection in GATE. *Rev. Geophys. Space Phys.*, **19**, 541–576.
- Intergovernmental Panel on Climate Change, 1995: *Climate Change 1995: The Science of Climate Change*, J. T. Houghton and B. A. Callendar, Eds., Cambridge University Press, 572 pp.
- Janowiak, J. E., and P. A. Arkin, 1991: Rainfall variations in the tropics during 1986–1989, as estimated from observations of cloud-top temperature. *J. Geophys. Res.*, **96**, 3359–3373.
- Krishnamurti, T. N., B. Jha, P. J. Rasch, and V. Ramanathan, 1997: A high resolution global reanalysis highlighting the winter monsoon. Part I: Reanalysis fields. *Meteor. Atmos. Phys.*, **64**, 123–150.
- Kulkarni, P. L., A. K. Mitra, S. G. Narkhedkar, A. K. Bohra, and S. Rajamani, 1997: On the impact of divergent part of the wind computed from INSAT OLR data on global analysis and forecast fields. *Meteor. Atmos. Phys.*, **64**, 61–82.

- Laing, A. G., and J. M. Fritsch, 1993: Mesoscale convective complexes over the Indian monsoon region. *J. Climate*, **6**, 911–919.
- Lopez, R. E., 1978: Internal structure and development processes of C-scale aggregates of cumulus clouds. *Mon. Wea. Rev.*, **106**, 1488–1494.
- Machado, L. A. T., M. Desbois, and J.-Ph. Duvel, 1992: Structural characteristics of deep convective systems over tropical Africa and the Atlantic Ocean. *Mon. Wea. Rev.*, **120**, 392–406.
- Mapes, B. E., and R. A. Houze Jr., 1993: Cloud clusters and superclusters over the oceanic warm pool. *Mon. Wea. Rev.*, **121**, 1398–1415.
- Moncrieff, M. W., and E. Klinker, 1997: Organized convective systems in the tropical western Pacific as a process in general circulation models: A TOGA COARE case-study. *Quart. J. Roy. Meteor. Soc.*, **123**, 805–827.
- Morcrette, J. J., 1991: Evaluation of model-generated cloudiness: Satellite-observed and model-generated diurnal variability of brightness temperature. *Mon. Wea. Rev.*, **119**, 1205–1224.
- Ramanathan, V., 1977: Interactions between ice-albedo, lapse-rate, and cloud-top feedbacks, an analysis of the nonlinear response of a GCM climate model. *J. Atmos. Sci.*, **34**, 1885–1897.
- , and W. Collins, 1991: Thermodynamic regulation of ocean warming by cirrus clouds deduced from observations of the 1987 El Niño. *Nature*, **351**, 27–32.
- Randall, D. A., P. Ding, and D.-M. Pan, 1997: The Arakawa–Schubert Parameterization. *The Physics and Parameterization of Moist Atmospheric Convection*, R. K. Smith, Ed., Kluwer Academic Publishers, 281–296.
- Redelsperger, J. L., 1997: The mesoscale organization of deep convection. *The Physics and Parameterization of Moist Atmospheric Convection*, R. K. Smith, Ed., Kluwer Academic Publishers, 59–98.
- Sadler, J. C., 1975: The monsoon circulation and cloudiness over the GATE area. *Mon. Wea. Rev.*, **103**, 369–387.
- Shemo, R. E., and J. L. Evans, 1996: Contributions of various classes of convection to rainfall in the Atlantic Ocean. *Meteor. Atmos. Phys.*, **60**, 191–205.
- Sikka, D. R., and S. Gadgil, 1980: On the maximum cloud zone and the ITCZ over Indian longitudes during the south west monsoon. *Mon. Wea. Rev.*, **108**, 1840–1853.
- Smith, E. A., and A. V. Mehta, 1990: The role of organized tropical storms and cyclones on intraseasonal oscillations in the Asian monsoon domain based on INSAT satellite measurements. *Meteor. Atmos. Phys.*, **44**, 195–218.
- Vintzileos, A., and R. Sadourny, 1997: A general interface between an atmospheric general circulation model and underlying ocean and land surface models: Delocalized physics scheme. *Mon. Wea. Rev.*, **125**, 926–941.
- Weare, B. C., and Coauthors, 1996: Evaluation of the vertical structure of zonally averaged cloudiness and its variability in the Atmospheric Model Intercomparison Project. *J. Climate*, **9**, 3419–3431.
- Webster, P. J., and G. L. Stephens, 1980: Tropical upper-tropospheric extended clouds—Inferences from winter MONEX. *J. Atmos. Sci.*, **37**, 1521–1541.
- Williams, M., and R. A. Houze Jr., 1987: Satellite-observed characteristics of winter monsoon cloud clusters. *Mon. Wea. Rev.*, **115**, 505–519.